


Research Article

Evaluation of the Crosswind Effect on the Horizontal Curve Safety on Rural Highways Using Vehicle Dynamic Simulation

Mohammad Yazdipour¹ and Ali Abdi Kordani² 

¹Department of Civil Engineering, Imam Khomeini International University, Qazvin, Iran

²Faculty of Civil Engineering, Imam Khomeini International University, Qazvin, Iran

Correspondence should be addressed to Ali Abdi Kordani; aliabdi@eng.ikiu.ac.ir

Received 17 July 2021; Revised 9 August 2021; Accepted 12 August 2021; Published 30 January 2022

Academic Editor: S. Mahdi S. Kolbadi

Copyright © 2022 Mohammad Yazdipour and Ali Abdi Kordani. This is an open access article distributed under the Creative Commons Attribution License, which permits unrestricted use, distribution, and reproduction in any medium, provided the original work is properly cited.

Horizontal curves, as one of the most accident-prone parts of the road, have always attracted special attention. When a vehicle is moving on a road, the driver has to be constantly on the lookout for small deviations from the main route, possibly due to disturbances such as wind, road roughness, and unwanted entrances by the driver. These types of deviations have a corrosive effect on the driver and will eventually lead to the overturning and slipping of vehicles, so they should be minimized. AASHTO standard procedures, as the most valid road design bylaw, do not consider the effect of lateral wind, in which the effect of lateral wind in arcs has been investigated in this research. The work conducted in this research is to increase knowledge about the directional stability of vehicles that are affected by strong winds and to investigate the parameters of the study using accurate models of dynamic simulation of vehicles that are subject to winds. This study aimed to increase the understanding of vehicle sensitivity to wind due to strong lateral winds. For this purpose, the process of passing different types of vehicles through horizontal arcs in different longitudinal slopes with different velocities of the vehicle under lateral wind is simulated and the mechanical properties of vehicles under such conditions are calculated to compare with the results obtained from the passage of vehicles through a smooth horizontal arc (without longitudinal slope) and without lateral wind. Overturning angle, slip angle, lateral acceleration, and lateral coefficient of friction of vehicles in this study were calculated through software outputs, and the effect of lateral wind on the safety of arcs has been investigated.

1. Introduction

Strong winds and storms are some of the natural disasters that cause a lot of damage in the world every year, including in Iran. Winds are classified into different categories based on the speed and impact they have on the sea surface. According to studies by the World Meteorological Organization, winds of more than 15 meters per second are known as storms. In the 1830s and 1840s, public transportation systems were used in most of Europe's major cities, and horse-drawn vehicles became commonplace in urban traffic. In the late nineteenth century, steam engines replaced electric motors, and eventually, internal combustion engines entered the market [1]. Figures 1 and 2 show an example of these changes in pressure. The aerodynamics of road vehicles is quite different from the aerodynamics of

aircraft. Three-dimensional airflow, unstable vibrations, and road surface all affect this process [3]. As the fluid passes through the surface, the velocity of the fluid also has properties such as those shown in Figure 1. Therefore, a vehicle passing under constant wind conditions has a constant speed ratio according to Figure 2 [2].

How the side wind affects the vehicle and how to apply it to identify existing weaknesses and errors will be investigated by studying books and articles written about calculating the radius of horizontal arcs in combination with longitudinal slopes, and then, the behavior of vehicles in the face of arcs combined with longitudinal slope and wind is investigated using vehicle dynamic simulator software [5]. Cars, trucks, and buses are the most widely used vehicles on the roads. Because of the importance of buses due to the large number of people in them and the high traffic on the

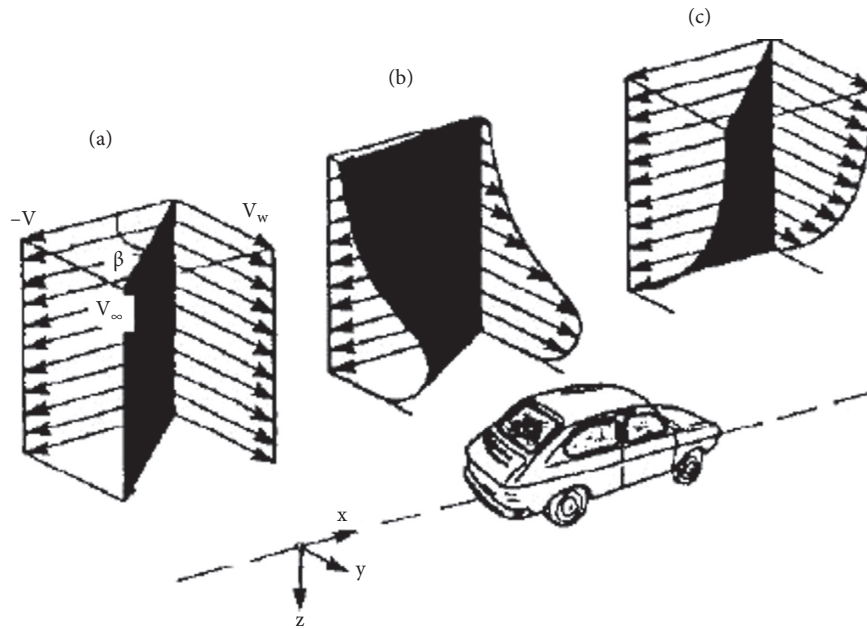


FIGURE 1: Comparison of artificial and natural speed characteristics [2].

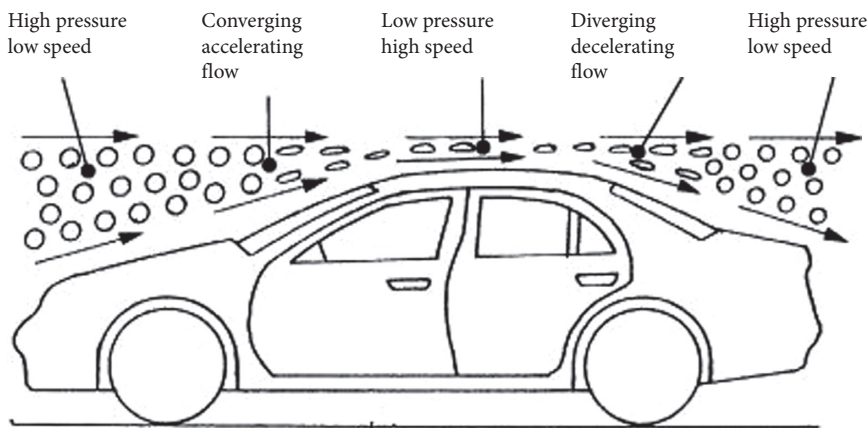


FIGURE 2: View of changes in pressure and velocity of the liquid passing through the car body [3].

roads, this issue was studied for this particular vehicle. However, research on passenger cars and trucks also raises our awareness.

1.1. Literature Review. Attention has recently been paid to the aerodynamic loads on vehicles in inverted motion conditions. An important feature of car roads is that they are usually located in large areas and as a result are exposed to wind [6]. The lateral wind model is based on the narrow-body theory, which examines the character of horizontal lateral wind velocity, in a 1973 study by Hochu and Amal Man. This model shows the lateral force and torque of inverted motion (Figure 3). This study showed how the lateral wind speed characteristic affects the size of the off-road and that relying solely on wind tunnel measurement when analysing sensitivity to strong winds will not be sufficient in Figure 4 [7]. In 1991, Ohno and Kohri investigated the effects of lateral air barriers on traction and lift

forces. They showed that traction and elevation can be reduced by zero lateral inversion through the lateral air barrier, but when the inverted angle is increased, elevation will also increase [8]. However, the rise can be reduced even in conditions of zero inverted movements by optimizing the shape of the lateral air barrier as shown in Figure 5 [9].

The models were also equipped with pressure transmitters that made it possible to analyse different types of pressure while creating movements during lateral winds [10]. They concluded that the transient reaction of the body with sharp parts can be detected by the formation and destruction of the separation bubble, leading to the achievement of the maximum amount of inverted torque. In addition, the creation of radii at sharp edges leads to an increase in constant inverse torque due to increased local pressures [11]. Ryan and Dominy [12] and Amundsen and Ranes [13] obtained the aerodynamic force of the passenger car model by overturning in the wind heading of about 30 [12, 13]. Fang [14] adjusted a vehicle dynamic simulation

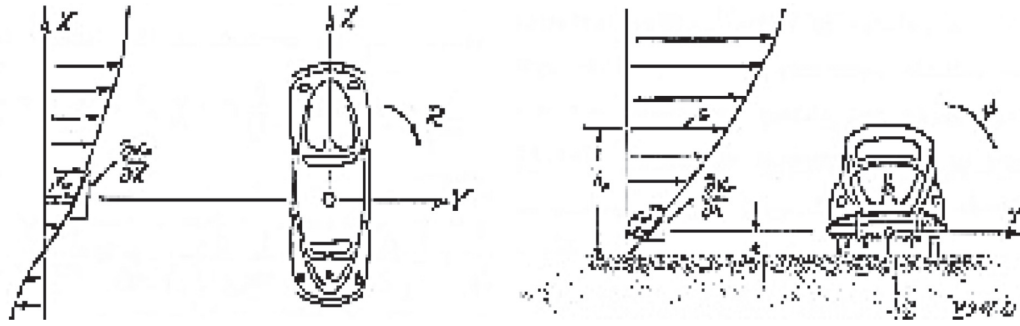


FIGURE 3: Characteristics of the opposite wind speed by Larabi and Hawk [6].

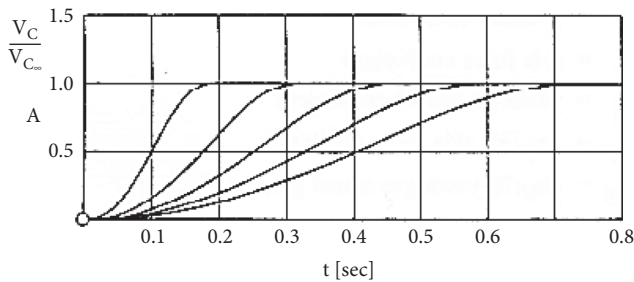


FIGURE 4: Lateral force coefficient and inverted torque due to strong wind [7].

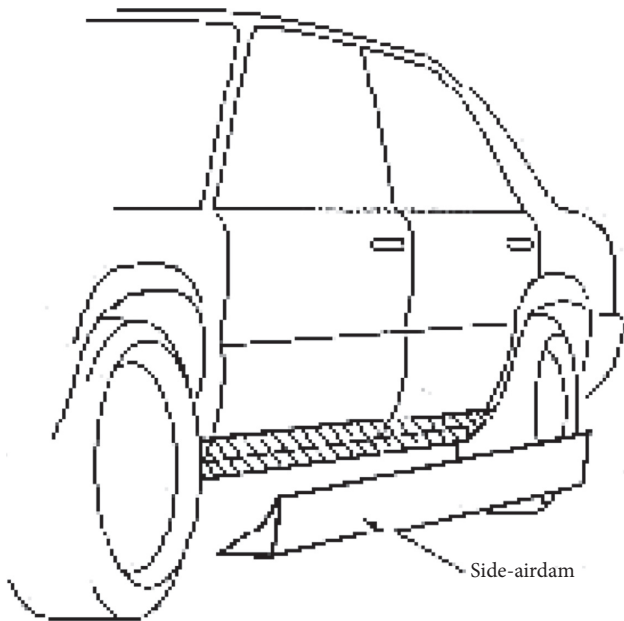


FIGURE 5: View of the lateral air barrier [9].

and model of high-speed aerodynamic characteristics and analysed the speed and the effects of lateral winds on vehicle displacement stability [14]. Maruyama and Yamazaki in 2006 examined the risk of an accident based on vehicle weight, tire load, aerodynamic force, and driving behavior, including strong mental behavior and other factors that are very difficult to determine [15]. Wu [16] studied the safety of highways affected by Typhoon climate and developed a car slip model. In addition, he calculated the speed of the car's safety stimulus under different degrees of Typhoon climate

but did not produce a quantitative wind response on paper [16]. Rodriguez and his colleagues (2014) used a stimulus simulator to measure the effect of opposite wind on driver behavior and vehicle lateral displacement and used a calculation model based on cross-cultural strength, driver behavior, and vehicle lateral displacement [17]. Zhou et al. [18] and Ueckermann et al. [19] studied the effect of opposite winds on design indices of alignment with wind tunnel testing but did not consider the effect of aerodynamic torque generated by wind and the unequal coefficient on the lateral stability of torques [18, 19].

2. Material and Methods

2.1. *The Geometry of the Route and Type of Vehicle.* The performance of vehicles in different geometric road conditions and at different speeds was evaluated to examine their stability against overturning and slipping. The design speeds of 40, 60, 80, 100, and 120 km/h, longitudinal slopes of -8%, -4%, 0, 4%, and 8%, and maximum design speed of 8% are considered. Besides, six side wind speeds were selected based on the World Meteorological Organization's classification. Therefore, the lateral winds of 0, 16, 34, 55, 80, and 111 km/h were selected. The minimum radius of the arcs is also used according to the AASHETO suggestion. Furthermore, the transition area with length L_r is considered to provide safe entry and exit of vehicles to the horizontal arcs [20]. Table 1 summarizes this explanation. In this study, a bus was selected [21]. The dimensional and mechanical specifications of vehicles are given in Table 2.

3. Results and Discussion

3.1. *The Coefficient of Friction along the Path in Different Modes.* Figure 6 shows the coefficient of lateral friction for the combination of $v = 80$ km/h and $g = -8\%$ along the path. In Figure 6, the coefficient of lateral friction in different parts of the path, including the initial straight path, circular arc, and straight end path, can be observed. The coefficient of friction is constant in the straight path until the start of the round application (beginning of L_r , station 41). During the round up to station 80 or the starting point of the arc, it increases to 0.05 due to the increase in lateral force in the positive direction. At the beginning of the arc, the lateral force changes direction due to the centrifugal force, so the lateral friction is reduced and this trend continues until the

TABLE 1: Bus specifications.

4490 mm	Length
2348 mm	Width
2920 mm	Height
1950 mm	Distance between wheels
6360 kg	Weight

TABLE 2: Path characteristics in the desired tests.

Lr (m)	L (m)	R (m)	V (km/h)
41	224.4	41	40
48	337.5	113	60
58	519.8	229	80
65	778.9	394	100

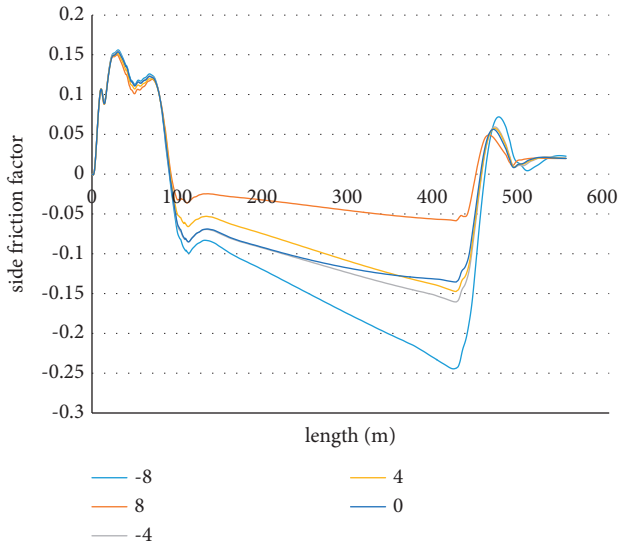


FIGURE 6: Comparison of coefficient of friction along the path at different slopes.

end of Lr (station 90) and reaches -0.18 . Then, it remains almost constant along the arc and at the endpoint of the arc (approximately station 257), and the friction jumps at once due to the disappearance of the centrifugal force and increases to the value of 0.055 . Then, l_r' has a decreasing trend by the end of it (station 295) due to the reduction in the existing lateral friction coefficient and reaches 0.01 . As can be observed, the trend of changes in the coefficient of friction in the case of lateral wind speed of 111 km/h is wider than other wind speeds. Therefore, as the lateral wind speed increases, the amount of friction increases due to the increase in lateral force. Figure 7 shows the coefficient of lateral friction available for the combination of $w = 34$ km/h and $v = 80$ km/h along the route.

As shown, the trend of changes in the coefficient of friction in the case of a slope of 8% is wider than that of other slopes. Therefore, the slope of -8% has the highest coefficient of friction and then the slope is -4% and the slopes of 0 and 4% are almost the same and the slope of 8% has the lowest coefficient of friction. The higher the coefficient of friction, the greater the road safety. Of course, it should be noted that Figure 7, despite the constant lateral wind, shows $w = 34$ km/h.

Figure 8 shows the coefficient of lateral friction available for the combination of $w = 34$ km/h and $g = -8\%$ along the path. As can be seen, the trend of changes in the coefficient of friction at a speed of 40 km/h has a higher coefficient of friction than that of other speeds, and as the speed increases, the coefficient of friction decreases, resulting in reduced safety.

Figure 9 shows the maximum values of the coefficient of friction on a slope of -4% for different wind speeds. According to Figure 9, the maximum value of the coefficient of friction at a speed of 40 km/h is for the time when there is no lateral wind, but at other speeds, the maximum value of the coefficient of friction is for the state where the lateral wind is its maximum value. For a side wind of 111 km/h, there are three data because the bus overturns at speeds of 100 and 120 km/h, and there are three data at a wind speed of 80 km/h because the car overturns when the speed is 120 km/h [22]. Table 3 shows the maximum values of the coefficient of friction, the percentage difference between them, the ground state at different speeds, and the wind speed of 16 km/h for the longitudinal slope state of -4% .

3.2. Analysing the Statistical Data of Friction Coefficient.

Since the value of the Kolmogorov–Smirnov is equal to 0.939 , the assumption that the residues are normal is confirmed. The second method can be observed from Figure 10, which confirms the assumption that the residues are normal. The third method is to use Figure 10 to achieve the normality of the residues. Therefore, the assumption that the residues are normal is confirmed. According to Figure 10, the variance of the residues is constant and its hypothesis is confirmed.

This hypothesis is confirmed using the Durbin–Watson test value. The statistical values of this test are between 0 and 4 , in which the values less than 1 will indicate positive correlations. The Durbin–Watson value of this model is 1.753 , so the assumption that the residues are uncorrelated is confirmed. As mentioned, this issue is referred to as the alignment problem in the statistical literature. The values of Vif and tolerance are used to investigate the presence or absence of alignment. Thus, if $Vif < 10$ and $tolerance > 0.1$, there is no alignment problem and the assumption of explanatory variables is confirmed. According to the values of Vif and tolerance, the assumption of explanatory variables is confirmed and the average value of residues is zero. Finally, the proposed model of maximum lateral friction in the horizontal arc for the bus is shown as follows:

$$f_y = 0.00003692 w^2 + 0.0000001 g^3 + 0.006 s - 0.601. \quad (1)$$

3.3. Lateral Acceleration along the Route in Various Modes.

Figure 11 shows the lateral acceleration for the combination of $v = 80$ km/h and $g = -8\%$ along the path. As shown, in the case where there is no lateral wind speed, the lateral acceleration is at its maximum and the lowest lateral acceleration is for the situation where the lateral wind is at its

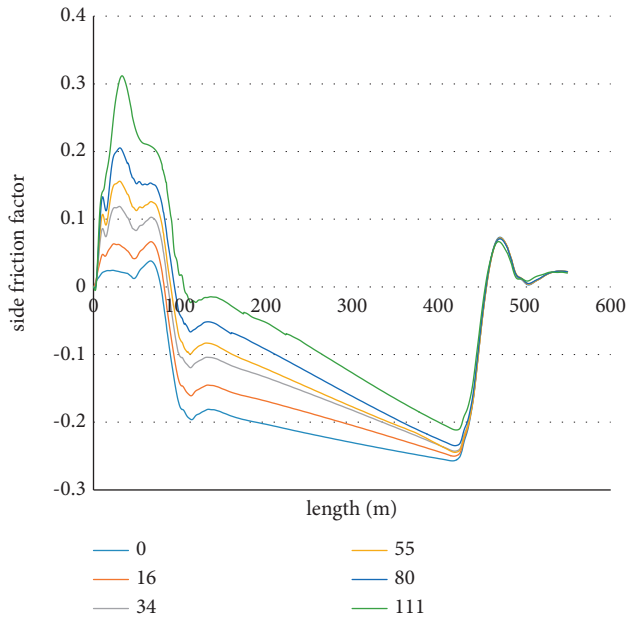


FIGURE 7: Comparison of coefficient of friction along the path at different wind speeds.

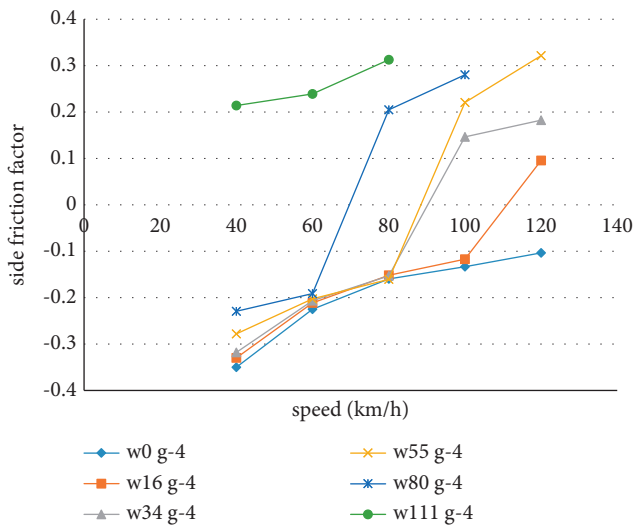


FIGURE 8: Comparison of maximum values of coefficient of friction.

maximum. Therefore, as the lateral wind decreases, the lateral acceleration also increases, which reduces road safety. Figure 12 shows the lateral acceleration for the combination of $w = 34$ km/h and $v = 80$ km/h along the route.

As shown, the -8% slope has the highest lateral acceleration and the 8% slope has the lowest lateral acceleration. Therefore, under constant lateral wind of 34 km/h, the slopes of -8% , -4% , 0% , 4% , and 8% have the highest lateral acceleration and the lowest safety, respectively. Figure 13 shows the lateral acceleration for the combination of $w = 34$ km/h and $g = -8\%$ along the path. As seen, the speed of 40 km/h has the highest lateral acceleration and the reason is because of its low radius, which also has the lowest safety compared with others. Therefore, the higher the speed, the

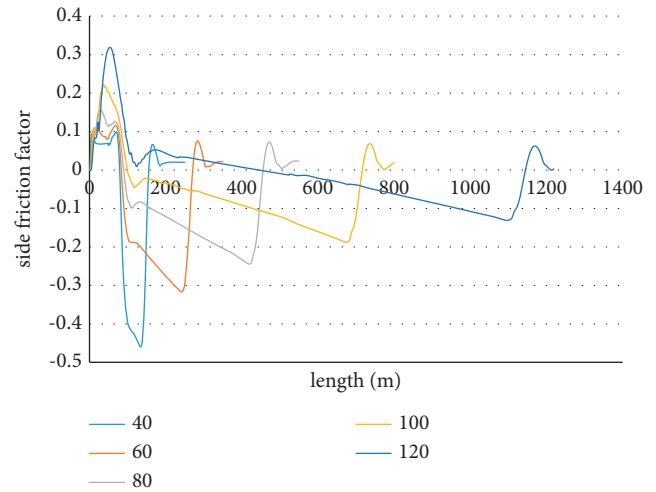


FIGURE 9: Comparison of the coefficient of friction along the route at different vehicle speeds.

TABLE 3: Percentage of changes in coefficient of friction on slope state of -4% and wind speed of 16 km/h.

Variation	Base value	W16 g-4	Speed
42.35	-0.23	-0.33	40
19.24	-0.18	-0.21	60
1.31	-0.15	-0.15	80
-11.68	-0.13	-0.12	100
-192.97	-0.10	0.10	120

lower the lateral acceleration and the greater the safety. Figure 14 shows the maximum values of lateral acceleration on a slope of -4% for different speeds.

Depending on the shape of the maximum lateral acceleration at speeds of 40 and 60 km/h, the lower the lateral wind, the more they are approximately equal at higher speeds. Table 4 shows the maximum lateral acceleration values, the percentage difference between them, the ground state at different speeds, and the wind speed of 16 km/h for the longitudinal slope state of -4% .

3.4. Analysing the Statistical Data of Lateral Acceleration.

First, considering that the value of the Kolmogorov-Smirnov is equal to 0.354 , the assumption that the residues are normal is confirmed. Second, Figure 15 shows that the assumption that the residues are normal is confirmed. The third method is to use Figure 15 to achieve the normality of the residues. Therefore, the assumption that the residues are normal is confirmed. According to Figure 15, it can be seen that the variance of the residues is constant and its hypothesis is confirmed.

This hypothesis is confirmed using the Durbin-Watson test value. The statistical values of this test are between 0 and 4 , in which the values less than 1 will indicate positive correlations. The value of the Durbin-Watson value of this model is equal to 1.534 , so the assumption that the residues are uncorrelated is confirmed. As mentioned, in the statistical literature, this issue is referred to as the alignment problem. The

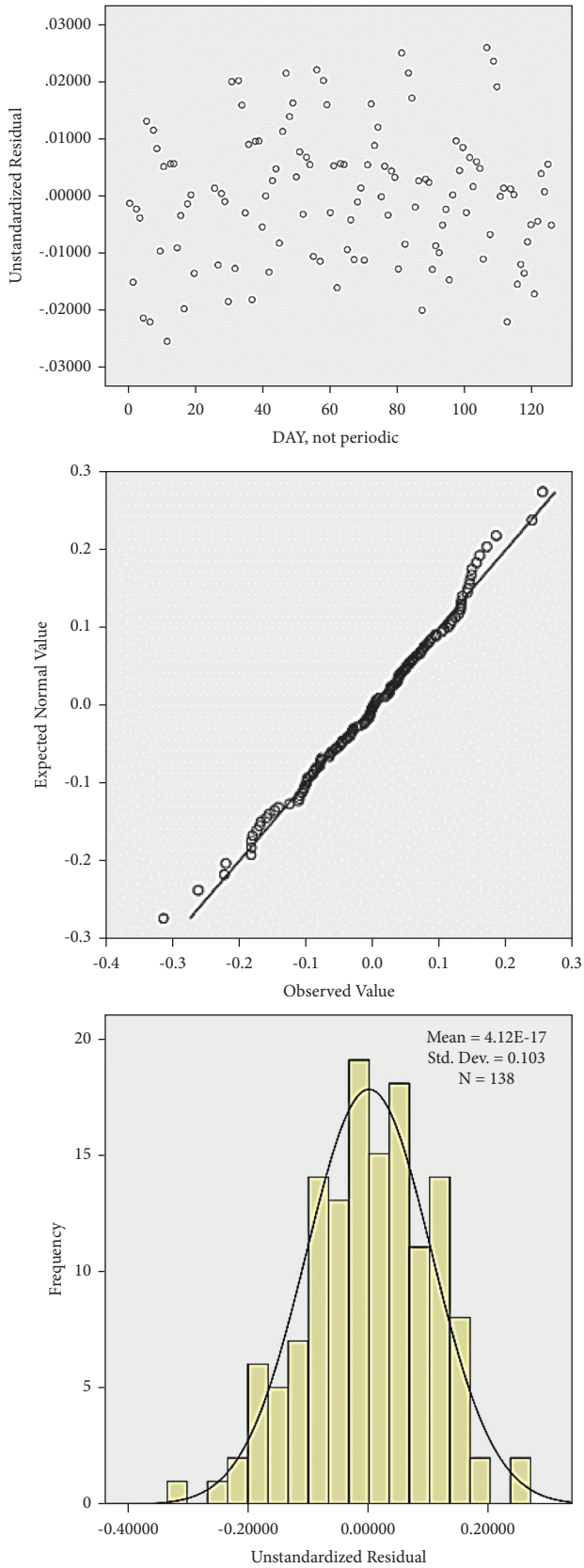


FIGURE 10: Histogram, quadratic diagram, and variance diagram of lateral friction coefficient model.

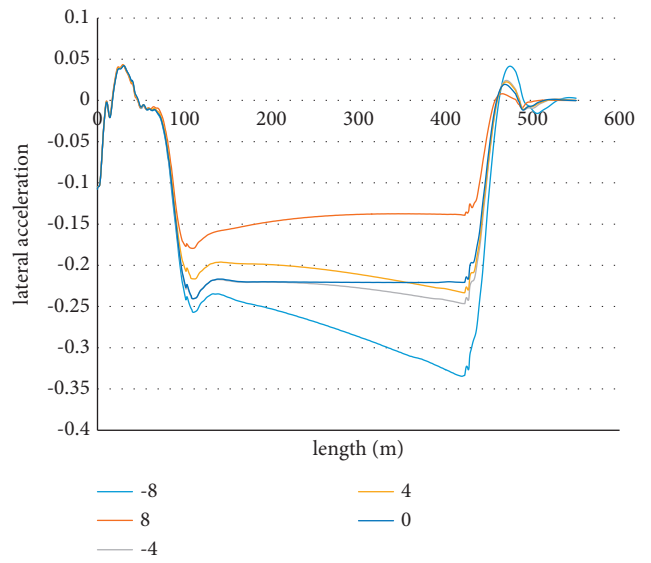


FIGURE 11: Comparison of lateral acceleration along the route on different slopes.

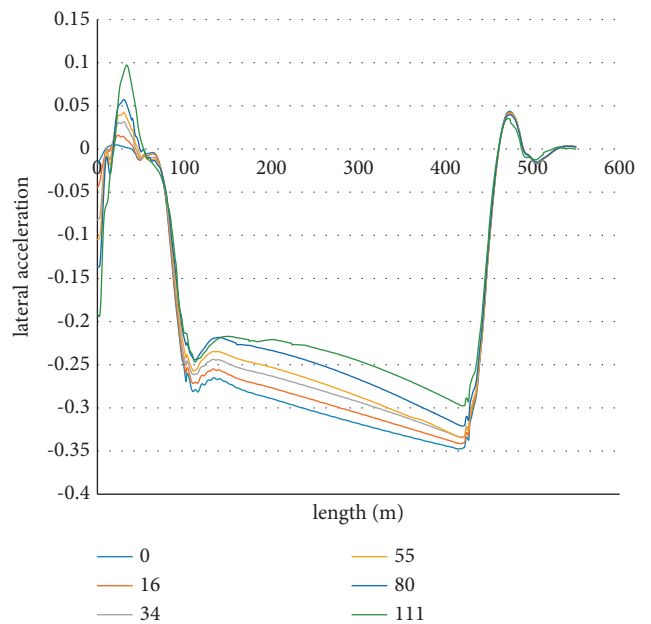


FIGURE 12: Comparison of lateral acceleration along the path at different wind speeds.

values of Vif and tolerance are used to explore the presence or absence of alignment. Thus, if $Vif < 10$ and $tolerance > 0.1$, there is no alignment problem and the assumption of noncorrelation of variables is confirmed. According to the values of Vif, the assumption of noncorrelation of variables is confirmed and the average value of residues is zero. Finally, the proposed model of maximum lateral acceleration in the horizontal arc for the bus is shown as follows:

$$a_y = -0.00001 w - 0.000001g^3 + 0.002 s - 0.451. \quad (2)$$

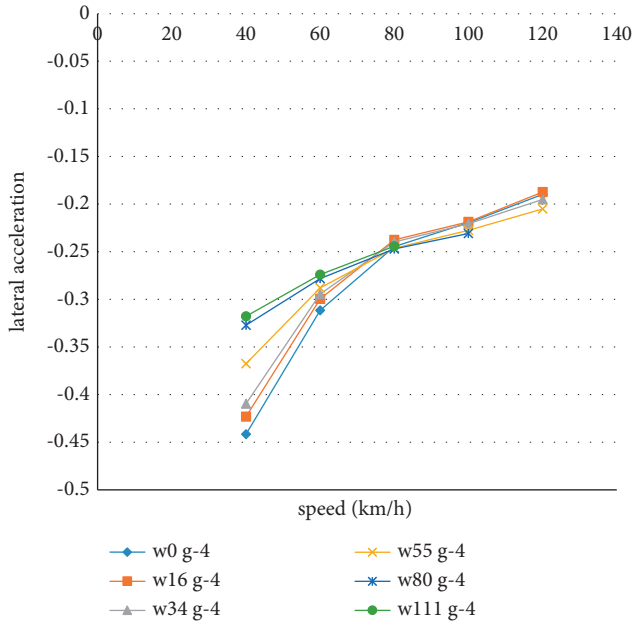


FIGURE 13: Comparison of maximum lateral acceleration values in terms of vehicle speed.

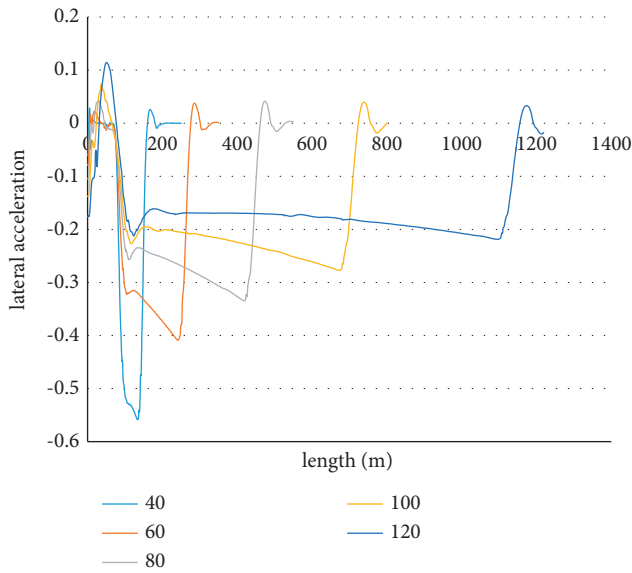


FIGURE 14: Comparison of lateral acceleration along the route at different vehicle speeds.

TABLE 4: Percentage of changes in lateral acceleration on slope state of -4% and wind speed of 16 km/h .

Variation	Base value	W16 g-4	Speed
34.54	-0.31	-0.42	40
13.79	-0.26	-0.30	60
1.15	-0.23	-0.24	80
-0.15	-0.22	-0.22	100
-0.79	-0.19	-0.19	120

3.5. *Overturning Angle along the Path in Different Modes.* Figure 16 shows the overturning angle for the combination of $v = 80\text{ km/h}$ and $g = -8\%$ along the path. As observed, in

the case of lateral wind speed of 111 km/h , the overturning angle is its maximum value and the lowest overturning angle is for the case where there is no lateral wind. Therefore, as the lateral wind increases, the overturning angle also increases, which reduces road safety. Figure 17 shows the reverse angle for the combination of $w = 34\text{ km/h}$ and $v = 80\text{ km/h}$ along the path.

As shown, the slopes of 0% , 4% , and -4% are almost the same, the highest overturning angle has 8% slope and -8% slope having the lowest overturning angle. Figure 18 shows the overturning angle for the combination of $w = 34\text{ km/h}$ and $g = -8\%$ along the path. As shown, the speed of 120 km/h has the highest overturning angle due to the high speed when entering the arc. Therefore, the higher the speed, the greater the overturning angle, resulting in lower safety. Figure 19 shows the maximum values of the overturning angle at a slope of -4% for different speeds.

According to Figure 19, at equal speeds, the higher the wind speed, the higher the maximum overturning angle. Table 5 shows the maximum values of the overturning angle, the percentage difference between them, the ground state at different speeds, and the wind speed of 16 km/h for the longitudinal slope state of -4% .

3.6. *Analysing the Statistical Data of Overturning Angle.* First, considering that the value of the Kolmogorov-Smirnov is equal to 0.442 , the assumption that the residues are normal is confirmed. The second method can be seen from Figure 20, which confirms the assumption that the residues are normal. Third, using Figure 20 can contribute to achieve the normality of the residues. Therefore, the assumption that the residues are normal is confirmed. According to Figure 20, the variance of the residues is constant and its hypothesis is confirmed.

This hypothesis is confirmed using the Durbin-Watson test value. The statistical values of this test are between 0 and 4 , in which the values less than 1 will indicate positive correlations. The Durbin-Watson value of this model is 2.048 , so the assumption that the residues are uncorrelated is confirmed. As mentioned, in the statistical literature, this issue is referred to as the alignment problem. The values of Vif are used to study the presence or absence of alignment. Thus, if $Vif < 10$ and $\text{tolerance} > 0.1$, there is no alignment problem and the assumption of uncorrelated variables is confirmed. According to the values of Vif, the assumption of explanatory variables is confirmed and the average value of residues is zero. Finally, the proposed model of maximum overturning angle in the horizontal arc for the bus is shown as follows:

$$\text{roll} = 0.00005406w^2 - 0.01g^2 + 1.526\text{logs} + 1.313. \quad (3)$$

3.7. *Slip Angle along the Path in Different Modes.* Figure 21 shows the slip angle for the combination of $v = 80\text{ km/h}$ and $g = -8\%$ along the path. In the case of lateral wind speed of 111 km/h , the slip angle is its maximum and the lowest slip angle is for the case where there is no lateral

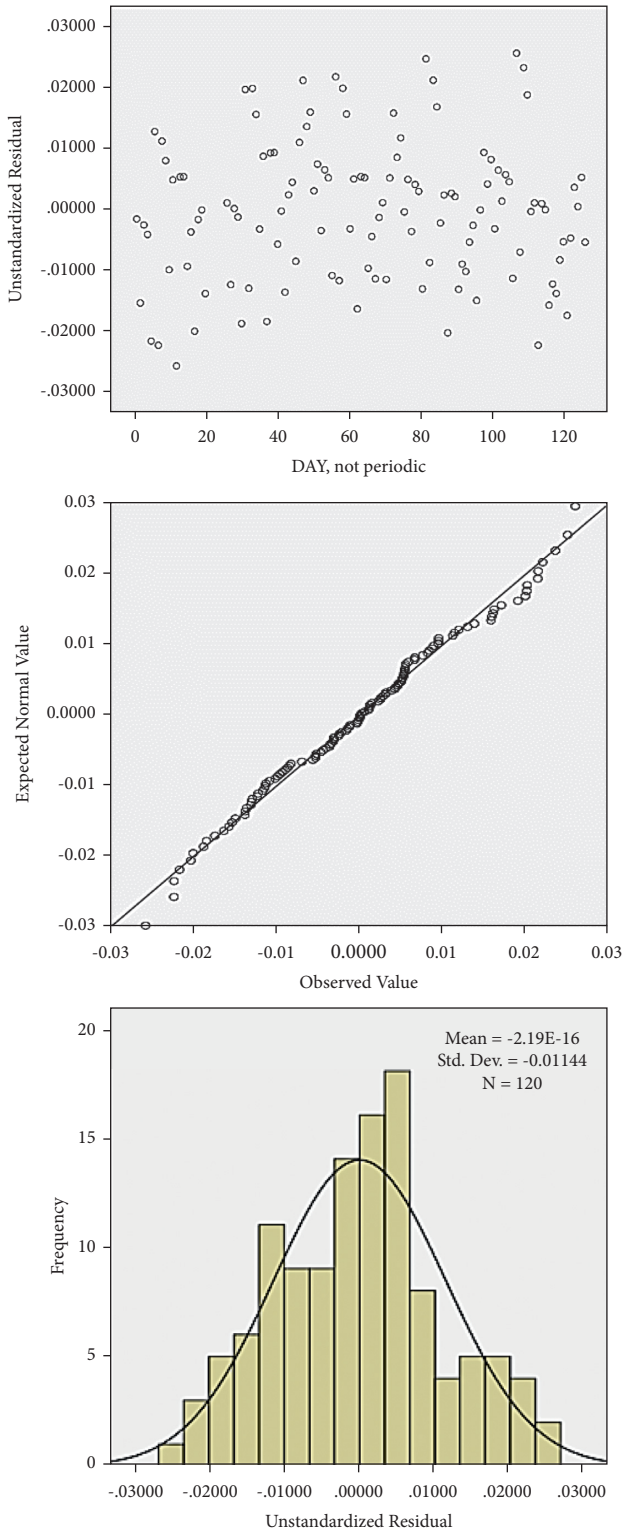


FIGURE 15: Histogram, quadratic diagram, and variance diagram of lateral acceleration model residues.

wind. Therefore, as the lateral wind increases, the slip angle also increases, which reduces road safety. Figure 22 demonstrates the slip angle for the combination of $w = 34$ km/h and $v = 80$ km/h along the path.

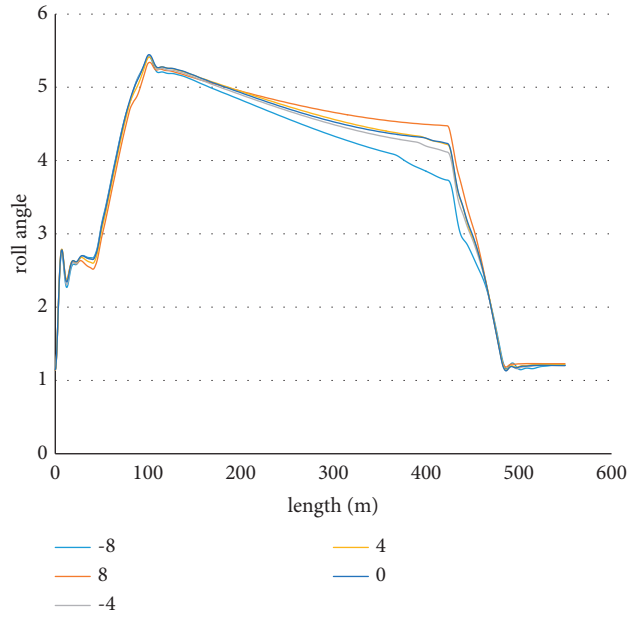


FIGURE 16: Comparison of overturning angle along the path on different slopes.

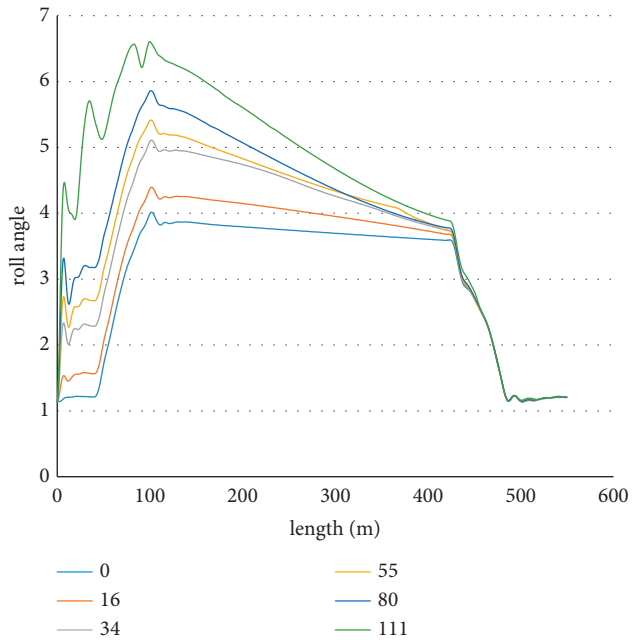


FIGURE 17: Comparison of overturning angle along the path at different wind speeds.

As can be seen, -8% slope has the highest slip angle and the 8% slope has the lowest slip angle. Therefore, under constant lateral wind of 34 km/h, the slopes of -8% , -4% , 0% , 4% , and 8% , respectively, have the highest slip angle and the lowest safety.

Figure 23 shows the slip angle for the combination of $w = 34$ km/h and $g = -8\%$ along the path. As can be seen in the bus, the speed of 120 km/h has the highest angle of slip, followed by the speeds of 60 , 80 , 40 , and 100 , respectively.

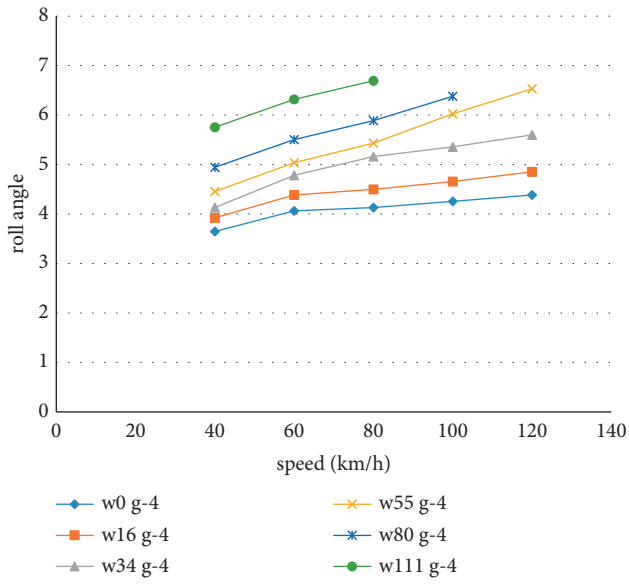


FIGURE 18: Comparison of maximum overturning angle values at different wind speeds.

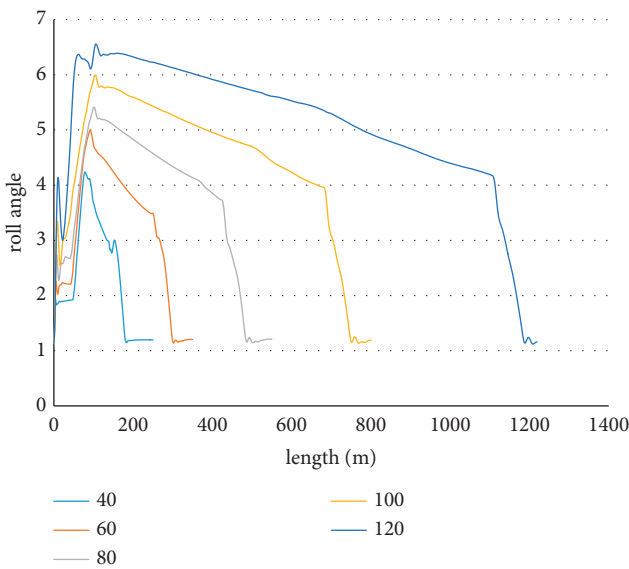


FIGURE 19: Comparison of overturning angle along the route at different vehicle speeds.

TABLE 5: Percentage of changes in overturning angle on slope state of -4% and wind speed of 16 km/h.

Variation	Base value	W16 g-4	Speed
0.39	3.90	3.92	40
5.94	4.14	4.39	60
7.59	4.18	4.50	80
8.62	4.29	4.66	100
10.05	4.41	4.85	120

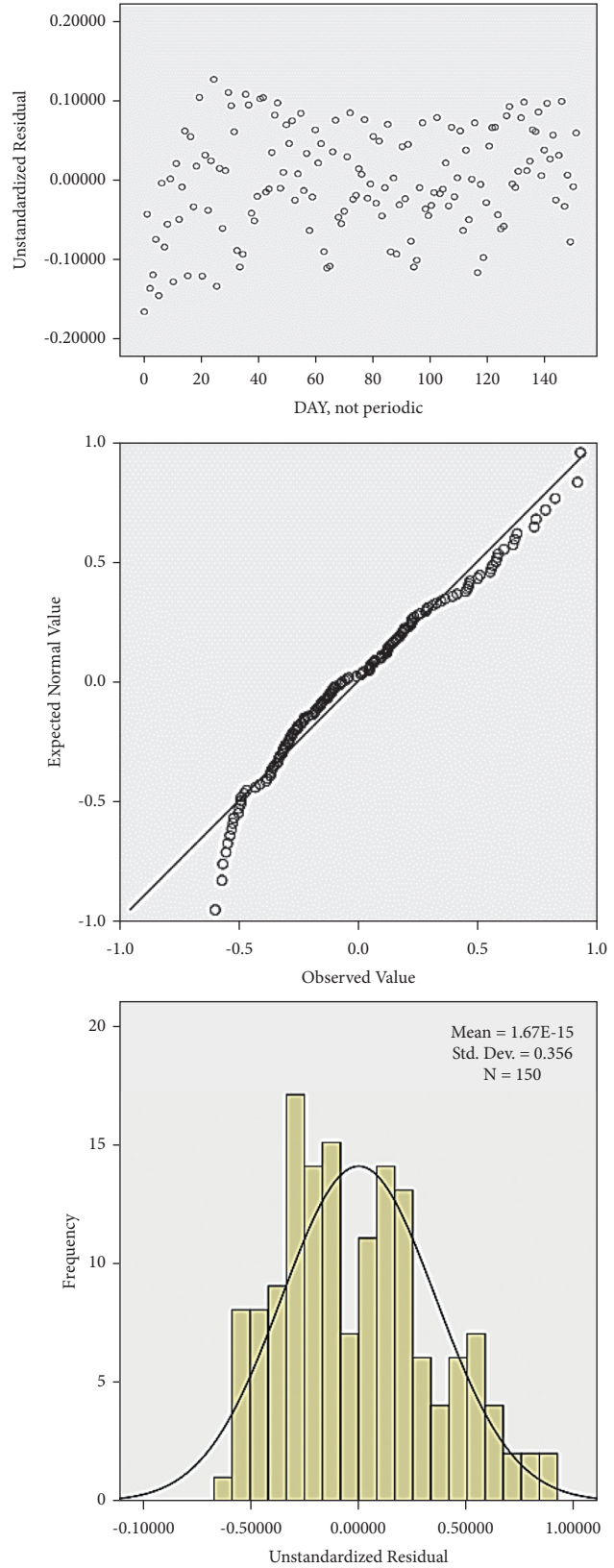


FIGURE 20: Histogram, quadratic diagram, and variance diagram of reverse angle model.

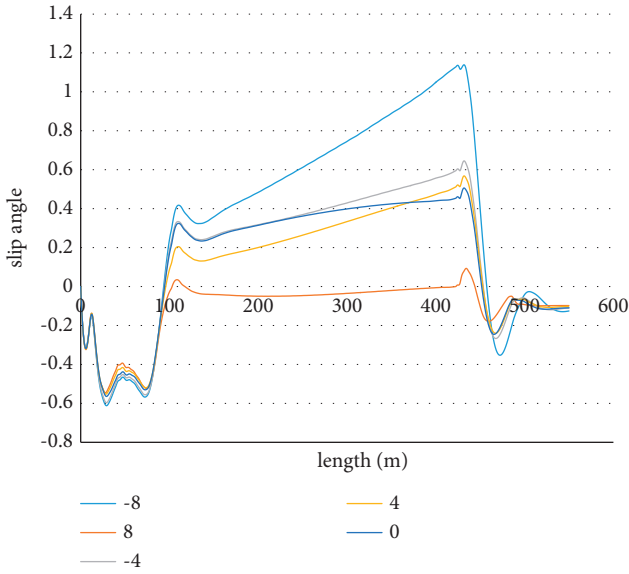


FIGURE 21: Comparison of slip angle along the path on different slopes.

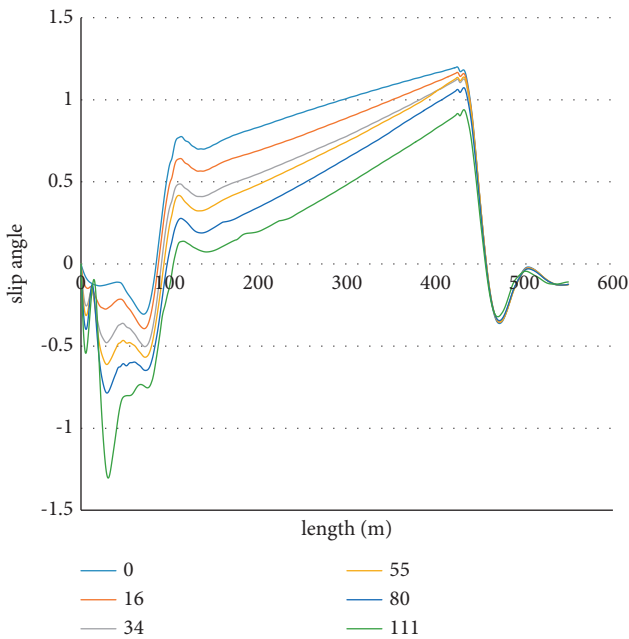


FIGURE 22: Comparison of slip angle along the path at different wind speeds.

Figure 24 shows the maximum slip angle values at a slope of -4% for different velocities. According to Figure 24 at equal speeds, the higher the wind speed, the higher the maximum slip angle. Table 6 shows the maximum values of the slip angle, the percentage difference between them, the ground state at different speeds, and the wind speed of 16 km/h for the longitudinal slope state of -4% .

3.8. *Analysing the Statistical Data of Slip Angle.* First, considering that the Kolmogorov-Smirnov value is equal to 0.2, the assumption that the residues are normal is

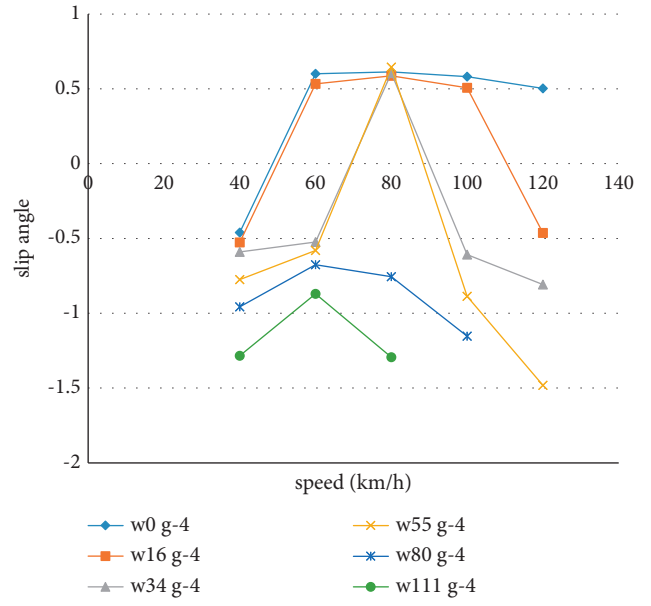


FIGURE 23: Comparison of maximum slip angle values in terms of vehicle speed.

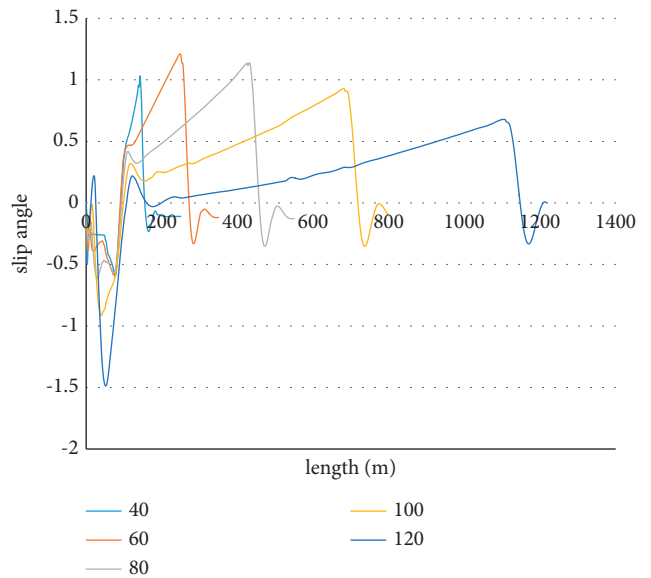


FIGURE 24: Comparison of slip angle along the route at different vehicle speeds.

TABLE 6: Percentage of changes in slip angle on slope state of -4% and wind speed of 16 km/h.

Variation	Base value	W16 g-4	Speed
-30.22	-0.76	-0.53	40
-242.23	-0.37	0.53	60
14.63	0.51	0.59	80
-11.06	0.57	0.51	100
-196.42	0.48	-0.46	120

confirmed. Second, Figure 25 shows that the assumption that the residues are normal is confirmed. Third, using Figure 25 contributes to achieve the normality of the residues. Therefore, the assumption that the residues are

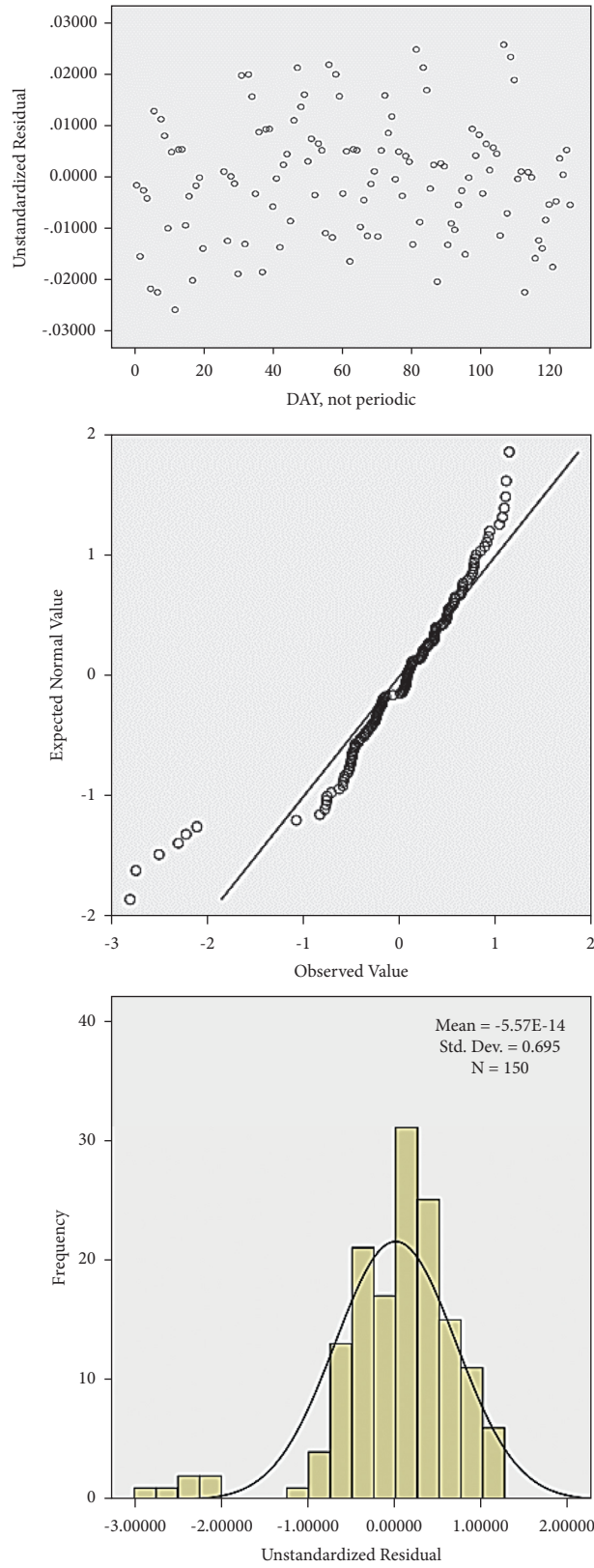


FIGURE 25: Histogram, quadratic diagram, and variance diagram of slip angle model in the horizontal arc for the bus.

normal is confirmed. According to Figure 25, the variance of the residues is constant and its hypothesis is confirmed.

This hypothesis is confirmed using the Durbin-Watson test value. The statistical values of this test are between 0 and 4, in which the values less than 1 will indicate positive

correlations. The Durbin–Watson value of this model is 1.509, so the assumption that the residues are uncorrelated is confirmed. As mentioned, in the statistical literature, this issue is referred to as the alignment problem. To investigate the presence or absence of alignment, the values of Vif and tolerance are used. Thus, if $Vif < 10$ and $tolerance > 0.1$, there is no alignment problem and the assumption of uncorrelated variables is confirmed. According to the values of Vif, the assumption of explanatory variables is confirmed and the average value of residues is zero. Finally, the proposed model of maximum slip angle in the horizontal arc for the bus is shown as follows:

$$slip = -0.004w + 0.0000001 g^3 - 82.273 \text{ inverse } s + 1.024. \quad (4)$$

4. Conclusion

In this research, the issue and the subject of the research were discussed and the necessity of conducting research was explained. Then, the questions and hypotheses were stated along with the main research objectives to clarify the details of the work. One of the highlights of this chapter is the effects of lateral winds on vehicle aerodynamics. In the following, the literature review has been discussed and an attempt has been made to collect and present a complete collection of researchers' studies on this subject. The studies of Mr Bowman, Takada, and Ohri, as well as Heyat and P, can be introduced as the most comprehensive studies in the field of lateral wind. Then, it gives a complete description of the method used for the research and explains the details of the study process. Accordingly, if the vehicle speed and longitudinal slope are constant, the existing lateral friction will increase as the lateral wind increases. For every 10 km/h increase in lateral wind, the lateral friction for each vehicle, SUV, bus, and two-axle truck increases by 3%, 13%, and 27%, respectively. Then, if the longitudinal slope and lateral wind intensity are constant, the existing lateral friction coefficient decreases as the vehicle speed increases. Per each 10 km/h increase in vehicle speed, the lateral friction for each vehicle, SUV, bus, and two-axle truck is reduced by 9%, 14%, and 17%, respectively.

If the lateral wind intensity and vehicle speed are constant, as the longitudinal slope shifts from uphill to downhill, the existing lateral friction coefficient increases; i.e., the longitudinal slope is 8% with the lowest available lateral friction coefficient and the longitudinal slope is -8% . The maximum available lateral friction coefficient is available. For every one percent increase in the longitudinal slope to the downside, the lateral friction for each vehicle, SUV, bus, and two-axle truck increases by 4, 5, and 6%, respectively. Accordingly, if the vehicle speed and longitudinal slope are constant, the lateral acceleration increases as the lateral wind increases. For every 10 km/h increase in lateral wind, the lateral acceleration for each vehicle, SUV, bus, and two-axle truck increases by 2, 3, and 5%, respectively. Accordingly, if the vehicle speed and longitudinal slope are constant, the overturning angle will increase as the lateral wind increases. For every 10 km/h increase in lateral wind, the overturning

angle for each vehicle, SUV, bus, and two-axle truck increases by 1.5%, 8%, and 12%, respectively. Furthermore, if the longitudinal slope and lateral wind intensity are constant, the overturning angle will increase as the vehicle speed increases. For every 10 km/h increase in vehicle speed, the overturning angle for each vehicle, SUV, bus, and two-axle truck is reduced by 2, 3, and 5%, respectively. Accordingly, if the vehicle speed and longitudinal slope are constant, the deviation rate increases as the lateral wind increases. For every 10 km/h increase in lateral wind, the deviation rate for each vehicle, SUV, bus, and two-axle truck increases by 1.5, 2.5, and 5%, respectively. Then, if the longitudinal slope and lateral wind intensity are constant, the deviation rate will decrease as the vehicle speed increases.

Data Availability

Requests for access to these data should be made to the corresponding author (email address: aliabdi@eng.ikiu.ac.ir)

Conflicts of Interest

The authors declare that there are no conflicts of interest regarding the publication of this study.

References

- [1] D. Cole, "Steering feedback mathematical simulation of effects on driver and vehicle," *Automobiltechnische Zeitschrift*, vol. 8, no. No.11-12, pp. 52–56, 2008.
- [2] W. H. Hucho, *Aerodynamics of Road Vehicles 4th Edition*, Cambridge University Press, Cambridge, United Kingdom, Article ID 0-7680-0029-7, 1998.
- [3] R. H. Barnard, *Road Vehicle Aerodynamic Design an Introduction*, Longman, Harlow, United Kingdom, 2nd edition, Article ID 0-9540734-0-1, 2001.
- [4] T. F. Brustad, "Preliminary studies on transition curve geometry: reality and virtual reality," *Emerging science journal*, vol. 4, no. 1, pp. 1–10, 2020.
- [5] S. M. Hashemian, A. Khodabakhshian, M. Gholipour, M. R. Esmaili, and M. Malekpour, "Approach for prediction of cold loads considering electric vehicles during power system restoration," *IET Generation, Transmission & Distribution*, vol. 14, no. 22, pp. 5249–5260, 2020.
- [6] W. D. Bowman, "Generalizations on the aerodynamic characteristics of sedan type automobile bodies," *SAE Technical Paper Series 660389*, vol. 37, 1966.
- [7] W. H. Hucho and H. J. Emmelmann, "Theoretical prediction of the aerodynamic derivatives of a vehicle in cross wind gusts," *SAE Technical Paper Series 730232*, vol. 2, 1973.
- [8] S.-M. Seyed-Kolbadi, M. Safi, K. Ayoub, S. M. S. Kolbadi, and M. Mirtaehri, "Explosive performance assessment of buried steel pipeline," *Advances in Civil Engineering*, vol. 2021, pp. 1–24, Article ID 6638867, 2021.
- [9] C. J. Baker, "Ground vehicles in high cross winds part I: steady aerodynamic forces," *Journal of Fluids and Structures*, vol. 5, no. 1, pp. 69–90, 1991.
- [10] S. Shadpoor, A. Pirouzi, H. Hamze, and D. Mazaheri, "Determination of Bodenstein number and axial dispersion of a triangular external loop airlift reactor," *Chemical Engineering Research and Design*, vol. 165, no. January 2021, pp. 61–68, 2021.

- [11] A. Chadwick, K. Garry, and J. Howell, "Transient aerodynamic characteristics of simple vehicle shapes by the measurement of surface pressures," *SAE Technical Paper Series 2001-01-0876*, vol. 10, 2001.
- [12] A. Ryan and R. G. Dominy, "The aerodynamic forces induced on a passenger vehicle in response to a transient crosswind gust at a relative incidence of 30," *SAE Technical Paper 980392*, vol. 13, pp. 1–11, 1998.
- [13] F. H. Amundsen and G. Ranes, "Studies on traffic accidents in Norwegian road tunnels," *Tunnelling and Underground Space Technology*, vol. 15, no. 1, p. 3e11, 2000.
- [14] G. Fang, *Research on Aerodynamic Characteristic of High Speed Automobile*, PhD Thesis, Hunan University, Changsha, 2000.
- [15] Y. Maruyama and F. Yamazaki, "Driving simulator experiment on the moving stability of an automobile under strong crosswind," *Journal of Wind Engineering and Industrial Aerodynamics*, vol. 94, no. 4, pp. 191–205, 2006.
- [16] J. X. Wu, *The Study of Safety Fore-Warning System of Freeway Based on the Typhoon Weather*, Master Thesis, Fujian Agriculture and Forestry University, Fuzhou, 2011.
- [17] J. M. Rodriguez, J. Codjoe, and O. Osman, "Experimental modeling of the effect of hurricane wind forces on driving behavior and vehicle performance," in *Proceedings of the Transportation Research Board 93rd Annual Meeting*, Washington DC, 2014.
- [18] H. Zhou, H. Kong, L. Wei, D. Creighton, and S. Nahavandi, "Efficient road detection and tracking for unmanned aerial vehicle," *IEEE Transactions on Intelligent Transportation Systems*, vol. 16, no. 1, pp. 297–309, 2014.
- [19] A. Ueckermann, D. Wang, and M. Oeser, "Calculation of skid resistance from texture measurements," *Journal of Traffic and Transportation Engineering: English Edition*, vol. 2, no. 1, p. 3e16, 2015.
- [20] S. M. S. Kolbadi, H. Piri, A. Keyhani, S. M. S. Kolbadi, and M. Mirtaheeri, "Seismic performance evaluation of slotted-web and bolt-flange plate moment connection," *Earthquakes and Structures*, vol. 20, no. 6, pp. 655–667, 2021.
- [21] R. T. Chen, S. Tang, T. Jansson, and J. Jansson, "A 45 cm long compression molded polymer-based optical bus," *Applied Physics Letters*, vol. 63, pp. 1032–1034, 1993.
- [22] L. Hu, G. Hong, J. Ma, X. Wang, and H. Chen, "An efficient machine learning approach for diagnosis of paraquat-poisoned patients," *Computers in Biology and Medicine*, vol. 59, pp. 116–124, 2015.